A double-beam piezo-magneto-elastic wind energy harvester for improving the galloping-based energy harvesting

A double-beam piezo-magneto-elastic wind energy harvester for improving the galloping-based energy harvesting

Kai Yang[1], Junlei Wang[2] *, Daniil Yurchenko[3]

[1] *School of Aerospace Engineering, Huazhong University of Science and Technology, Wuhan 430074, China*
[2] *School of Mechanical and Power Engineering, Zhengzhou University, Zhengzhou 450000, China*
[3] *Institute of Mechanical, Process & Energy Engineering, Heriot-Watt University, Edinburgh EH14 4AS, UK*

Abstract

This study investigates the performance of a double-beam piezo-magneto-elastic wind energy harvester (DBPME-WEH) when exhibiting galloping-based energy harvesting regime under a wind excitation. The DBPME-WEH comprises two piezoelectric beams, each of which supports a prism bluff body embedded with a magnet at the tip. The magnets are oriented to repulse each other to introduce bistable nonlinearity. Wind tunnel tests were conducted to compare performances of the DBPME-WEH and a double-beam piezoelectric wind energy harvester (DBP-WEH) that doesn't comprise the magnet-induced nonlinearity. The results reveal that compared to the DBP-WEH, the critical wind speed to activate the galloping vibration of DBPME-WEH can be reduced up to 41.9 %. Thus, the results corroborate the significant performance enhancement by the DBPME-WEH. It can be also found that the distance of the two magnets affects the performance, and the distance that achieves the weakly bistable nonlinearity is beneficial to energy harvesting in reducing the critical wind speed and improving the output voltage.

Wind energy harvester (WEH) can transduce the wind-induced structural vibration into electric power. Since wind is ubiquitous in natural environment, the WEH can be widely applied, which has drawn great attentions in recent years [1-5]. Various measures can be employed to enhance performance of a single WEH, e.g., an application of concurrent vibration sources[3, 6-7], aerodynamic shape optimization [8-16], optimization of the shunted circuit [17-23] and utilization of the fluid vortex [24-28]. It can be found that most previous researches focused on the fluid-solid coupling mechanisms between the wind and a linearly modelled structure. While these measures can successfully improve the performance of WEH, there still exists a potential to improve the energy harvesting performance if the linear structure is replaced. It was reported that the magnet-induced nonlinearity can bring significant improvement for a variety of mechanical systems, e.g., mechanical vibration energy harvester [29-33] and low-frequency broadband vibration isolator [34, 35]. Therefore, the benefit of the magnet-induced nonlinearity encouraged a few researchers to introduce this type of nonlinearity into WEH for performance enhancement [36-39]. For example, Bibo et al. [36] discussed influence of the different types of a magnet-induced nonlinearity on a single galloping-based WEH. The experimental results validated that the significant performance enhancement can be realized if the appropriate type of the magnet-induced nonlinearity is used. Alhadidi and Daqaq [37] demonstrated the improvement of the lock-in region of a single wake-galloping WEH by using a magnet-induced nonlinearity. Naseer et al. [38] proposed a monostable piezo-magneto-elastic energy harvester for vortex-induced vibrations. Attractive magneto-static force was employed to bring

* Author to whom correspondence should be addressed. Email: jlwang@zzu.edu.cn

the monostable nonlinearity, and the simulation results corroborated the performance improvement in terms of the bandwidth and efficiency. Zhou et al. [39] proposed a Y-shaped bistable energy harvester to scavenge the low speed wind energy, where the bistable nonlinearity is implemented by a tip magnet and two fixed magnets. The experimental results proved that the snap-through and reach coherence resonance are beneficial to energy harvesting enhancement.

Although the above studies revealed the advantage of the magnet-induced nonlinearity in WEH, they have only concentrated on a single-beam wind energy harvesting structure and none of them have considered the magnet-induced nonlinearity for the double-beam energy harvester. A double-beam energy harvester is a structure comprising two piezoelectric beams, and thus the vibration energy of each beam can be harvested, which can saliently generate more power than the single-beam energy harvester. When adding the magnets into the double-beam energy harvester, each magnet is supported by a beam. Consequently, the magnet interaction of both the vibrating magnets subjected to an external excitation produces energy transmission between both the beams. The magnetic interaction of the two vibrating magnets provides an additional disturbance apart from the wind excitation, which may increase the likelihood of activating the galloping vibrations subjected to a low-speed wind excitation. This may lead to far more different dynamic behaviors under a wind excitation from the single piezo-magneto-elastic energy harvester, studied in Refs. [36-39] (where only one of the magnets can vibrate and others are fixed). The energy transmission between two elastically supported magnets was once reported in performance improvement of mechanical vibration energy harvesters under base excitations [40, 41]. However, the physical mechanism of a mechanical vibration energy harvester (which is a forced vibration system) is much different from a wind energy harvester (which is a parametrically excitation system[10]). Thus, it is worthy to uncover the performance improvement and the physical connotation of a double-beam WEH using the magnet-induced nonlinearity through wind tunnel experiments.

This study proposes a double-beam piezo-magneto-elastic wind energy harvester (DBPME-WEH), which remained uninvestigated, and intends to perform the wind tunnel tests to investigate the performance of DBPME-WEH when exhibiting galloping vibration. Fig. 1 presents the schematic of the DBPME-WEH, the photo of the experimental setup and the bi-stable static equilibrium positions of each beam, respectively. The DBPME-WEH comprises two cantilever beams (material: China GBT 65Mn structural steel, and denoted by the 1st and 2nd beams, respectively), each of which supports a prism-like bluff body (material: foam) embedded with a magnet (material: neodymium iron boron, $5 \times 5 \times 5$ $(\text{mm})^3$) at the tip. The two magnets repulse each other to produce magnet-induced nonlinearity into the WEH. The magnet-induced nonlinearity would become stronger along with reducing the distance between the two magnets Δ. Consequently, the magnetostatic force buckles both the beams to produce the bistable nonlinearity. That is, bi-stable static equilibrium positions of each beam on the either side of the center line can be discovered. The experiments are conducted in an open-circuit circular-section wind tunnel with a diameter of 400 mm. Two identical piezoelectric transducers (material: PZT-5, capacitance: $C_p = 26$ nF, internal resistor: $R \approx 1$ MΩ) are attached on the roots of both the beams to transduce the beam vibration into voltage, respectively. The digital oscilloscope (Model: DS1104S, RIGOL., China) is used to acquire the voltage output of the piezoelectric transducers. To eliminate the influence of the static voltage bias in the oscilloscope, in the following figures, the standard deviations of the voltage outputs of the piezoelectric transducers are presented. Table 1 lists the geometrical parameters of the beams and piezoelectric transducers. It is seen that the 2nd beam is thicker than the 1st beam, while the lengths and widths of them are identical. This indicates that the 2nd beam is stiffer than the 1st beam when no magnets are installed. The total masses of the 1st beam and the 2nd beam with the piezoelectric transducers are 3.75×10^{-3} Kg and 4.65×10^{-3} Kg, respectively. The mass of each the bluff body embedded with the magnet is 2.72×10^{-3} Kg.

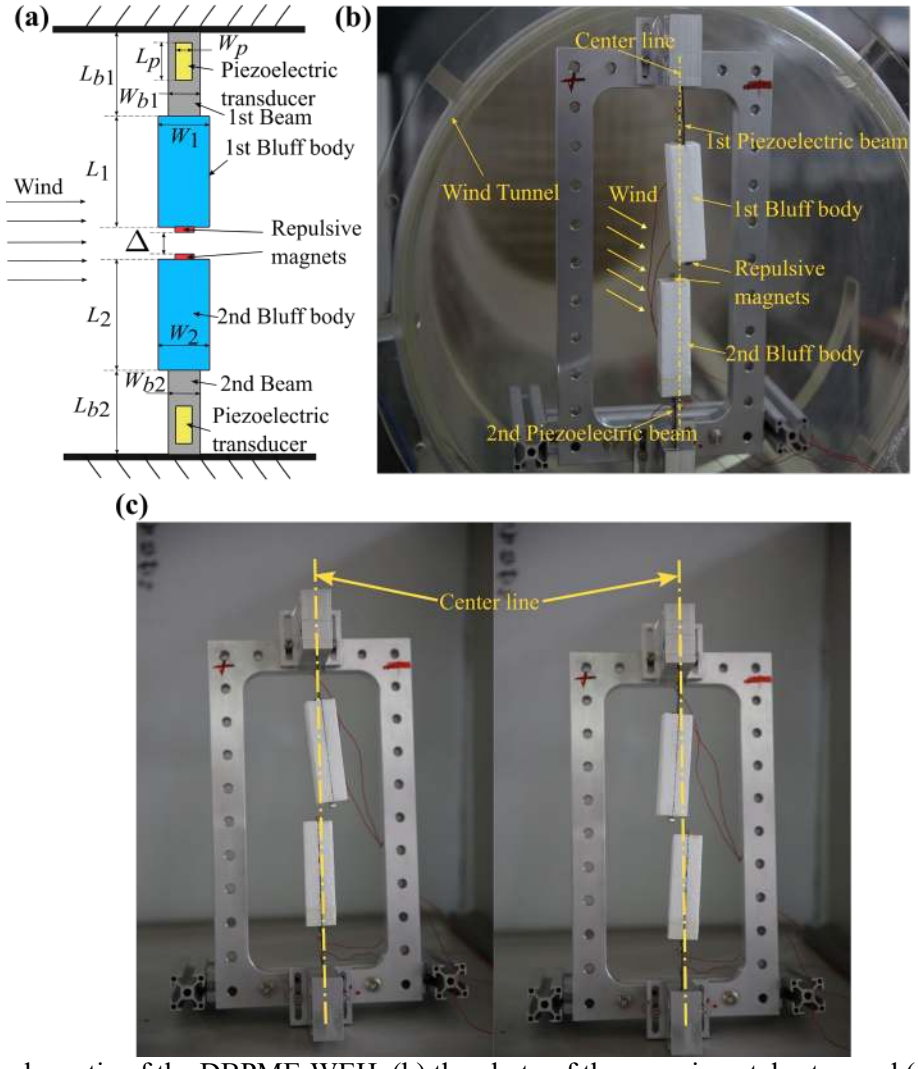

Fig. 1 (a) The schematic of the DBPME-WEH, (b) the photo of the experimental setup and (c) the bi-stable static equilibrium positions of each beam

Table 1 The geometric parameters of the beams and piezoelectric transducers of the DBPME-WEH

Description	Value (mm)
1st beam: Length (L_{b1}) × Width (W_{b1}) × Thickness	$45 \times 20 \times 0.15$
2nd beam: Length (L_{b2}) × Width (W_{b2}) × Thickness	$45 \times 20 \times 0.2$
1st bluff body: Length (L_1) × Width (W_1) × Thickness	$85 \times 24 \times 24$
2nd bluff body: Length (L_2) × Width (W_2) × Thickness	$85 \times 24 \times 24$
Piezoelectric transducer: Length (L_p) × Width (W_p) × Thickness	$30 \times 10 \times 0.4$

To show the advantages of the magnet-induced nonlinearity for performance enhancement, Figs. 2 and 3 present the voltage output standard deviations of the 1st and 2nd beams of the DBPME-WEH and

the double-piezoelectric wind energy harvester (DBP-WEH) (which replaces both the magnets with the identical-weight nonmagnetic mass, respectively). Due to the wind tunnel property, the wind excitations with the following discrete speeds are provided (reserving a decimal fraction): [1.5, 1.7, 1.8, 2.0, 2.1, 2.2, 2.4, 2.5, 2.6, 2.8, 2.9, 3.1, 3.2, 3.3, 3.5, 3.6, 3.7, 3.9] m/s. In this experiment, the distance of the magnets of the DBPME-WEH is $\Delta = 18$ mm, where the weakly bistable nonlinearity is realized. The absolute value of the average static equilibrium position of the 1st beam is $|x_{eq}| = 4.5$ mm, and the absolute value of the average static equilibrium position of the 2nd beam is $|y_{eq}| = 1.25$ mm. The critical speed is defined to be the smallest wind speed that can activate the galloping vibration of the beam. That is, the smaller the critical speed, the better the wind energy harvesting performance. Fig.2 shows that for the 1st beam, the critical speed of the DBPME-WEH is 1.8 m/s, reduced by 25% (i.e., $(2.4 - 1.8)/2.4 \times 100\%$) compared to the DBP-WEH (2.4 m/s). Increasing the wind speed leads to a larger voltage output of the 1st beam of both the DBPME-WEH and the DBP-WEH. Fig. 3 shows that the critical speed of the DBP-WEH 2nd beam is significantly greater than that of the 1st beam. Since the 2nd beam is thicker than the 1st beam in the experiment (as shown in Table 1), and consequently the 2nd beam is stiffer than the 1st beam. According to Tang et al. [42], it was discovered that for the cantilever beam that supports a bluff body, it is easier for the softer beam to exhibit the galloping-based vibration compared to the stiffer beam. Hence, the critical wind speed of the 2nd beam (stiffer beam) of the DBP-WEH is greater than that of the 1st beam (softer beam). However, the critical speed of the DBPME -WEH 2nd beam is the same as the 1st beam, which is reduced by 41.9 % compared to the 2nd beam of the DBP-WEH. It is found that the critical speeds of the two beams of the DBPME-WEH are same due to the interaction of the two magnets at the tips of both the bluff bodies. Once the galloping vibration of the 1st beam (the softer beam) is activated under the low-speed wind excitation, the vibrating magnet of the 1st beam will produce an excitation force (i.e., variable magnetic repulsion force of the two magnets) that leads to vibration of the tip of the 2nd beam's bluff body. As a result, the vibration of the 2nd beam is also activated, which consequently generates voltage. Overall, the results in Figs. 2 and 3 verify the significant performance enhancement by using the magnet-induced nonlinearity for galloping-based energy harvesting of the double-beam structure.

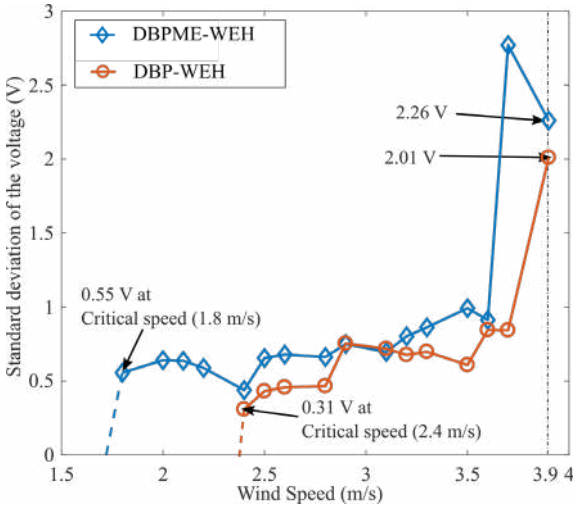

Fig. 2 The voltage output standard deviations of the 1st beam of the DBPME-WEH and DBP-WEH with respect to different wind speeds

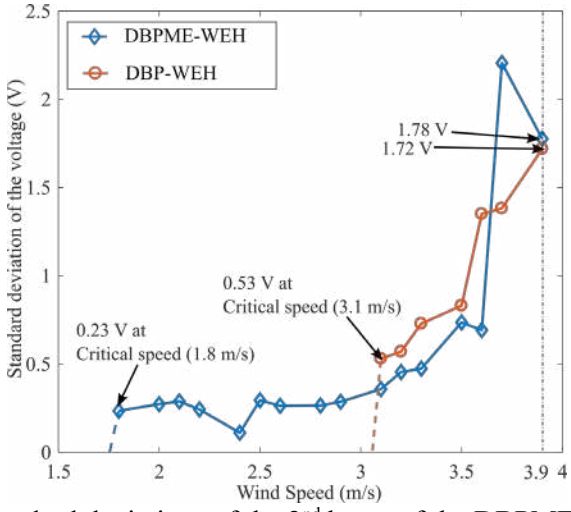

Fig. 3 The voltage output standard deviations of the 2nd beam of the DBPME-WEH and DBP-WEH with respect to different wind speeds

The magnet-induced bistable nonlinearity is strengthened when the two magnets become closer. It is curious to show the influence of the magnet-induced bistable nonlinearity on the performance of the DBPME-WEH, so as to develop the insights into effective DBPME-WEH design. Therefore, this study performs the experiments of the DBPME-WEH with three different distances of the two magnets. Fig.2 presents the schematics of the beam buckled by the magnetic interaction for $\Delta = [6, 12, 18]$ mm, respectively. It is seen that when Δ is smaller, the magnet-induced bistable nonlinearity is strengthened, as expected, where the level of buckling both the beams is enhanced. Hence, equilibrium positions become further way from the center line for the smaller distance Δ.

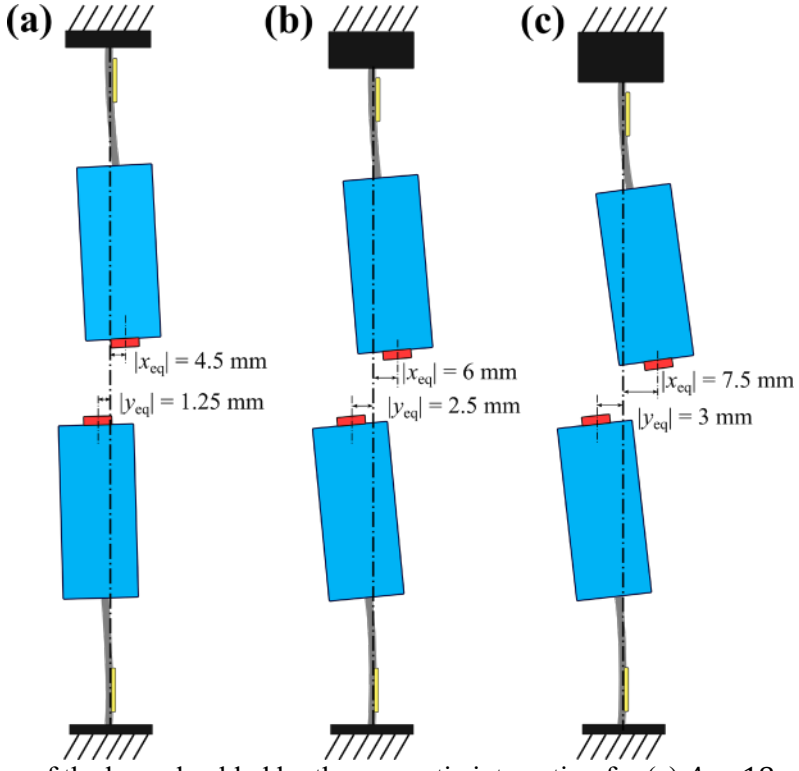

Fig. 4 The schematics of the beam buckled by the magnetic interaction for (a) $\Delta = 18$ mm; (b) $\Delta = 12$ mm; (c) $\Delta = 6$ mm

Figs. 5 and 6 present the voltage output standard deviations of the 1st and 2nd beams of the DBPME-WEH for $\Delta = [6, 12, 18]$ mm. As shown in Fig.5, the critical speed of the 1st beam approaches 2.2 m/s for the smaller distance $\Delta = 6$ mm and $\Delta = 12$ mm, which is greater than the critical speed for $\Delta = 18$ mm (1.8 m/s). It is seen that increasing the wind speed can lead to output voltage improvement of the DBPME-WEH for the three distances Δ. It is also seen that the largest voltage output at 3.9 m/s degrades significantly when the distance of the two magnets are smallest. As shown in Fig.6, although the 2nd beam is stiffer than the 1st beam, it can be also found that the critical speed approaches 2.2 m/s for the smallest considered distances $\Delta = 6$ mm and $\Delta = 12$ mm, and the voltage at the largest wind speed 3.9 m/s in the experiment significantly declines corresponding to the decreasing distance between two magnets. The critical speeds for $\Delta = 6$ mm and $\Delta = 12$ mm may have a small deviation. However, since the wind tunnel can only provide the wind excitations with discrete speeds, the deviation of the critical speeds for $\Delta = 6$ mm and $\Delta = 12$ mm is smaller than the increment of the wind speeds in the experiment. Consequently, the deviation is unable to be shown in the Figs. 5 and 6. The results show that the variation trend of the 2nd beam output voltage in terms of the distance is similar to the 1st beam. Therefore, for both the beams, it can be concluded that the weakly magnet-induced bistable nonlinearity (i.e., the larger distance) is beneficial to the performance of the DBPME-WEH.

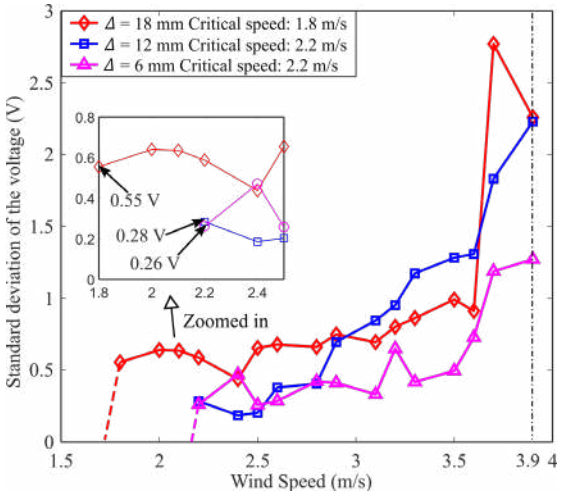

Fig. 5 The voltage output standard deviations of the 1st beam of the DBPME-WEH for $\Delta = [6, 12, 18]$ mm with respect to different wind speeds

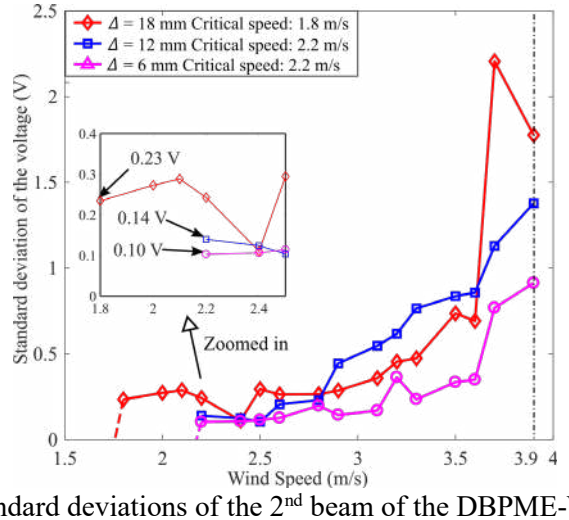

Fig. 6 The voltage output standard deviations of the 2nd beam of the DBPME-WEH for $\Delta = [6, 12, 18]$ mm with respect to different wind speeds

The change of the critical speeds can be qualitatively interpreted by the formulae of the magnet-induced bistable nonlinearity. For the DBPME-WEH, the restoring forces of the two beams when considering the approximate model of the magnet-induced nonlinear force[31,35,40] can be expressed as follows:

$$F_1 = (k_1 + k_{b1})x_1 - k_{b1}x_2 + k_{b3}(x_1 - x_2)^3 \quad (1)$$

$$F_2 = (k_2 + k_{b1})x_2 - k_{b1}x_1 + k_{b3}(x_2 - x_1)^3 \quad (2)$$

where x_i is the displacement of the tip of the bluff body supported by the ith beam. $k_i > 0$ is the equivalent stiffness at the tip of the bluff body supported by the ith beam without the magnets, when only considering the beam's fundamental mode. $k_{b1} < 0$ and $k_{b3} > 0$ are the negative linear stiffness and positive cubic nonlinear stiffness of the magnet-induced nonlinear force, respectively. $|k_{b1}|$ and $|k_{b3}|$ become larger when the magnets are closer to each other[31,35,40]. The equivalent total linear stiffness terms of the 1st and 2nd beams are $(k_1 + k_{b1})$ and $(k_2 + k_{b1})$, respectively. Note that, the negative linear stiffness k_{b1} counterbalances the positive linear stiffness $k_i (i = 1,2)$. For an appropriate distance of the two magnets, the equivalent total linear stiffness terms $(k_1 + k_{b1})$ and $(k_2 + k_{b1})$ may be of small magnitude. Thus, according to Tang et al.[42], the critical speed is significantly decreased due to the reduction of the linear stiffness. When further reducing the magnet distance (i.e., increasing the value of

$|k_{b1}|$ and $|k_{b3}|$), the absolute values of the equivalent total linear stiffness $|k_1 + k_{b1}|$ and $|k_2 + k_{b1}|$ rise and consequently the critical speeds of both the beams are increased. For the situation where $|k_{b1}|$ is far greater than the beam stiffness k_i due to the small distance of the magnets (e.g. $\Delta = 6$ mm and $\Delta = 12$ mm), the influence of the beam stiffness k_i is slight, and thus the magnet interaction becomes dominant, (i.e., $F_1 \approx k_{b1}(x_1 - x_2) + k_{b3}(x_1 - x_2)^3$ and $F_2 \approx k_{b1}(x_2 - x_1) + k_{b3}(x_2 - x_1)^3$). In this manner, the DBPME-WEH behaves as a system that two bluff bodies are only supported by the magnets. As a result, changing the distance of the magnets may only affect the static stable positions of the bluff bodies, instead of the critical speed.

In summary, this study proposes a double-beam piezo-magneto-elastic wind energy harvester (DBPME-WEH) and investigates its performance through a wind tunnel experiment. The DBPME-WEH utilizes the magnet-induced bistable nonlinearity to enhance the energy harvesting performance. The experimental results show that the DBPME-WEH significantly outperforms the double-piezoelectric wind energy harvester (DBP-WEH) that is lack of the magnet-induced nonlinearity. That is, the critical wind speed to activate the galloping vibrations of the 1st beam and 2nd beam (stiffer beam) of the DBPME-WEH are respectively reduced by 25% and 41.9 %. The experimental studies also reveal that larger distance between the two magnets, which achieves the weakly bistable nonlinearity, is favorable for the performance of the DBPME-WEH in reducing the critical wind speed and enhancing the output voltage.

This work was supported by National Natural Science Foundation of China (Grant No.: 11802097, 51977196 and 51606171).

[1] J. Zhang, J. Zhang, C. Shu, and Z. Fang, Appl. Phys. Lett. **110**, 3 (2017).

[2] H. Zou, L. Zhao, Q. Gao, L. Zuo, F. Liu, T. Tan, K. Wei, and W. Zhang, Appl. Energy **255**, 113871 (2019).

[3] Z. Lai, J. Wang, C. Zhang, G. Zhang, and D. Yurchenko, Energy Convers. Manag. **199**, 111993 (2019).

[4] X. He, X. Yang, and S. Jiang, Appl. Phys. Lett. **112**, 033901 (2018).

[5] V.J. Ovejas and A. Cuadras, Smart Mater. Struct. **20**, 085030 (2011).

[6] H Dai, A. Abdelkefi, and L. Wang, Nonlinear Dyn. 77, 967 (2014).

[7] L. Zhao, H. Zou, G. Yan, F. Liu, T. Tan, K. Wei, and W. Zhang, Energy Convers. Manag. **201**, 112166 (2019).

[8] J.M. Kluger, F.C. Moon, and R.H. Rand, J. Fluids Struct. **40**, 185 (2013).

[9] A. Abdelkefi, Z. Yan, and M.R. Hajj, J. Intell. Mater. Syst. Struct. **25**, 246 (2013).

[10] G. Hu, K.T. Tse, K.C.S. Kwok, J. Song, and Y. Lyu, Appl. Phys. Lett. **109**, 193902 (2016).

[11] G. Hu, K.T. Tse, M. Wei, R. Naseer, A. Abdelke, and K.C.S. Kwok, Appl. Energy **226**, 682 (2018).

[12] J. Wang, S. Zhou, Z. Zhang, and D. Yurchenko, Energy Convers. Manag. **181**, 645 (2019).

[13] G. Hu, K.T. Tse, and K.C.S. Kwok, Appl. Phys. Lett. **108**, 123901 (2016).

[14] J. Song, G. Hu, K.T. Tse, S.W. Li, and K.C.S. Kwok, Appl. Phys. Lett. **111**, 223903 (2017).

[15] Y. Yang, L. Zhao, and L. Tang, Appl. Phys. Lett. **102**, 064105 (2013).

[16] J. Wang, L. Tang, L. Zhao, and Z. Zhang, Energy **172**, 1066 (2019).

[17] L. Zhao, L. Tang, and Y. Yang, J. Intell. Mater. Syst. Struct. **27**, 453 (2016).

[18] L. Zhao and Y. Yang, Sensors Actuators, A Phys. **261**, 117 (2017).

[19] T. Tan and Z. Yan, AIP Adv. 7, 035318 (2017).

[20] S. Zhou, J. Cao, D.J. Inman, S. Liu, W. Wang, and J. Lin, Appl. Phys. Lett. **106**, 093901 (2015).

[21] S. Zhou, J. Cao, A. Erturk, and J. Lin, Appl. Phys. Lett. **102**, 173901 (2013).

[22] K. Fan, Q. Tan, Y. Zhang, S. Liu, M. Cai, and Y. Zhu, Appl. Phys. Lett. **112**, 123901 (2018).

[23] Z. Chen, J. He, J. Liu, and Y. Xiong, IEEE Trans. Power Electron. **34**, 2427 (2019).

[24] S. Zhou and J. Wang, AIP Adv. **8**, 075221 (2018).

[25] L. Zhang, H. Dai, A. Abdelkefi, and L. Wang, Appl. Phys. Lett. **111**, 073904 (2017).

[26] A. Abdelkefi, J.M. Scanlon, E. McDowell, and M.R. Hajj, Appl. Phys. Lett. **103**, 033903 (2013).

[27] M. Usman, A. Hanif, I.H. Kim, and H.J. Jung, Energy **153**, 882 (2018).

[28] G. Hu, J. Wang, Z. Su, G. Li, H. Peng, and K.C.S. Kwok, Appl. Phys. Lett. **115**, 073901 (2019).

[29] K. Yang, F. Fei, and H. An, Nonlinear Dyn. **96**, 2369 (2019).

[30] D. Huang, S. Zhou, and G. Litak, Nonlinear Dyn. **97**, 663 (2019).

[31] W. Cai, and R. L. Harne, Smart Mater. Struct. **28**, 075040 (2019).

[32] Z. Zhou, W. Qin, and P. Zhu, Mech. Syst. Sig. Proc. **84**, 158 (2017).

[33] G. Wang, W. -H. Liao, Z. Zhao, J. Tan, S. Cui, H. Wu, and W. Wang, Nonlinear Dyn. **97**, 2371 (2019).

[34] B. Yan, H. Ma, W. Zheng, B. Jian, K. Wang, and C. Wu. IEEE-ASME T. Mech. **24**, 1851 (2019).

[35] K. Yang, R. L. Harne, K. W. Wang, and H. Huang, Smart Mater. Struct. **23**, 045033 (2014).

[36] A. Bibo, A. H. Alhadidi, and M. F. Daqaq, J. Appl. Phys. **117**, 045103 (2015).

[37] A. H. Alhadidi and M. F. Daqaq, Appl. Phys. Lett. **109**, 033904 (2016).

[38] R. Naseer, H.L. Dai, A. Abdelkefi, and L. Wang, Appl. Energ. **203**, 142(2017).

[39] Z. Zhou, W. Qin, P. Zhu, and S. Shang, Energy, **153**, 400 (2018).

[40] C. Lan, L. Tang, W. Qin, and L. Xiong, J. Intel. Mat. Syst. Str. **29**, 1216 (2018).

[41] M. S. Nguyen, Y. -J. Yoon, O. Kwon, and P. Kim, Appl. Phys. Lett. **111**, 253905 (2017).

[42] L. Tang, L. Zhao, Y. Yang, and E. Lefeuvre, IEEE-ASME T. Mech. **20**, 834 (2015).